MODELLING OF FLOW PAST BODY WITH THICK WAKE IN CLASSICAL AIR WING THEORY

F. TOISON, Ph. LEGALLAIS, J. HUREAU

Laboratoire de Mécanique et d'Energétique
Ecole Supérieure de l'Energie et des Matériaux - Université d'Orléans
Rue Léonard de Vinci 45072 ORLEANS Cédex 2 - FRANCE

1. Introduction

Since the precursor works of Helmholtz and Kirchhoff, the theory of the two dimensional potential flow of an incompressible ideal fluid has been very extensively developed in hydrodynamics and aerodynamics. This can be explained by the fact that the powerful methods of complex function theory are applicable. Since Joukowsky's theorem, the motion of an airfoil with constant circulation is well known. Now, owing to the fondamental works of Couchet[3] and Mudry[12] on vortex sheets complemented by numerical conformal mapping, an exact solution to the unsteady motion of wing with continuous shedding of vortices from the trailing edge is available. Moreover the profile may be deformable during the motion. Computed values of hydrodynamics forces present a good agreement with experimental results. So, the theory of thin wake wing can be considered as achieved in 2D flow.

The problem of thick wake modelling is different. Helmholtz used a « dead zone » running indefinitely behind the obstacle with a constant pressure equal to the free stream pressure. This flow pattern was very popular in the beginning of this century as it provided a way of getting around d'Alembert's paradox, so that the drag could be calculated. Levi-Civita[10] and Villat[16] elaborated the mathematical foundations of this model. Later, Leray[11] showed the existence and uniqueness of the solution to this flow, but, unfortunately, the velocity field and the free streamlines can be determined only for extremely simple cases (flat plate, wedge and circular arcs). The theory then fell into disuse for some time. At the beginning of the fifties, using the increasing capacities of computers, results for cylinders, arcs, and plates with split flap, are computed by Birkhoff and Zarantonello[2], and Wu[18]. Lastly, in 1986 Elcrat and Trefethen[5] studied polygonal bodies and obstacles approximated by polygonal lines, using a numerical treatment of the modified Schwarz-Christoffel integral.

This paper presents a general numerical method that provides the solution for an obstacle of arbitrary geometry[8]. The results obtained show that the Helmholtz wake theory can predict lift and pressure distribution as long as it is used with a boundary layer computation to specify the position of the separation points. Because Cp is null in the wake, the drag coefficients we compute are underestimated. So we propose a new model called « virtual wall » model[9], which should predict the drag as well as the lift. Now the pressure in the wake is not equal to the free stream one and its value must be determined by computing the forces applied to the obstacle. This model is more complicated than the first one because it calls for a solution to a mixed problem of the function theory. The flow is then analyzed and described without reference to experimental data. For each model, we have tested the accuracy of the results of our programs, and computed the values of C_D and C_L for various bodies.

2. Helmholtz's Model

An obstacle of known geometry is placed in an infinite stream of velocity V_∞, parallel to the x-axis, and of pressure P_∞. $\mathcal{P}$ is the wetted wall, A is the upstream infinite point, and D is the stagnation point. C and E are the points where the flow separates from $\mathcal{P}$, and $\mathcal{L}_{CB}$ and $\mathcal{L}_{EF}$ are the free streamlines coming from C and E (Fig (2.I)).

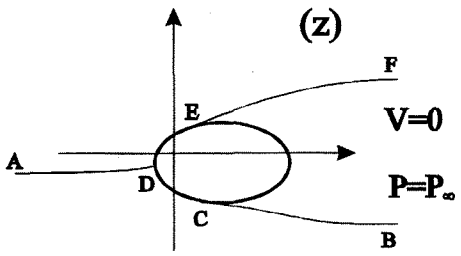

Fig (2.I)

Let f(z) be the complex potential and its derivative w(z) the complex velocity.
The boundary conditions are :

$$\lim_{z\to\infty} w(z) = V_\infty \qquad (2.1)$$

$$\mathrm{Im}\{w(z)dz\} = 0 \quad \text{on } \mathcal{P} \qquad (2.2)$$

$$|w(z)| = V_\infty \quad \text{on } \mathcal{L}_{CB} \text{ and } \mathcal{L}_{EF} \qquad (2.3)$$

The locations of points C and E used to be obtained by Brillouin's conditions. In fact, a boundary layer analysis can only calculate the location of the current break-away points. We shall therefore assume that points C and E are specified.

2.1 Theoretical Formulation

Here, the problem cannot be solved by calculating dz = df/w where f and w are obtained by conformal mapping, because the w-plane is unknown. The function Ω defined by the following relations, must be considered.

$$\Omega = i\log\frac{w}{V_\infty} = \Theta + iT$$

where Θ is the angle the fluid velocity makes with the x-axis, and T is given by : $|\vec{V}| = V_\infty e^T$.

This is a mixed problem for Ω, because Θ is known on $\mathcal{P}$, and T = 0 on ℓ_{CD} and ℓ_{EF}.

The mixed problem becomes a Dirichlet problem by use of the Levi-Civita method: The domain of the f-plane is mapped on the inside of the upper unit semi-disk Δ^+, in the ζ-plane Fig (2.II), in such a way that the free streamlines map onto the diameter. Since T = 0 on the diameter, the function can then, according to Schwarz's principle of symmetry, be continued analytically across the diameter on the whole disk Δ and the mixed problem then becomes a Dirichlet problem. If $\theta(\sigma) = \Theta(e^{i\sigma})$ (Villat's function) is supposed to be known on the boundary of Δ, the Schwarz-Villat formula can be used to determine Ω and consequently $\tau(\sigma) = T(e^{i\sigma})$. From (2.1) $\Omega(0) = 0$, so the constant of the formula is null and Ω is easily calculated:

$$\Omega(\zeta) = \frac{1}{\pi}\int_0^\pi \frac{1-\zeta^2}{1-2\zeta\cos(\sigma)+\zeta^2}\theta(\sigma)\,d\sigma \qquad (2.4)$$

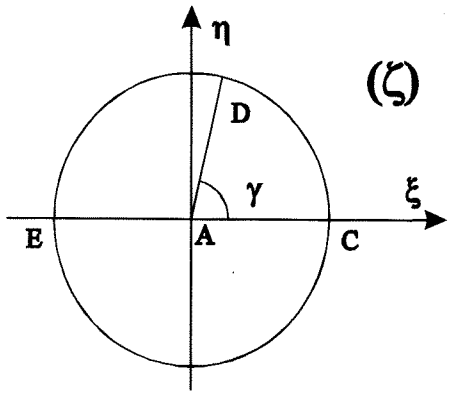

Fig (2.II)

Now, f-plane must be mapped on ζ-plane. The diagrams in the different planes used are shown in figure (2.III).

The classical transformations are:

$$* f = a^2(Z+\cos\gamma)^2 \quad \text{with}$$

$$a = \frac{\sqrt{\varphi_E}+\sqrt{\varphi_C}}{2} \quad \text{and} \quad \cos\gamma = \frac{\sqrt{\varphi_E}-\sqrt{\varphi_C}}{\sqrt{\varphi_E}+\sqrt{\varphi_C}}$$

where φ_C and φ_E are the velocity potential values at C and E, and the value $\zeta = e^{i\gamma}$ corresponds to point D.

$$* Z = -\frac{1}{2}\left(\zeta+\frac{1}{\zeta}\right)$$

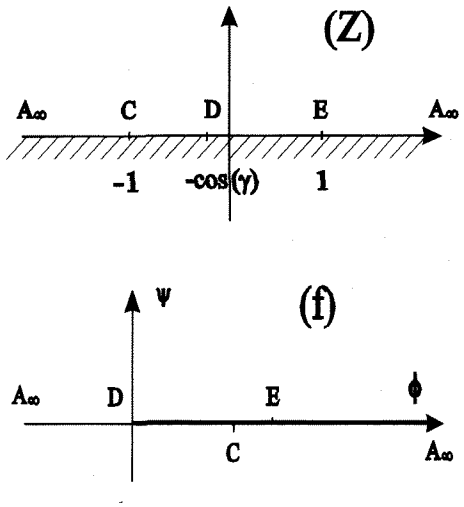

Fig (2.III)

Finally we obtain:

$$f = a^2\left[\cos(\gamma) - \frac{1}{2}\left(\zeta+\frac{1}{\zeta}\right)\right]^2 \qquad (2.5)$$

Since φ_C and φ_E are unknown, a and γ are constants to be determined.

$$dz = \frac{df}{w} \text{ gives :}$$

$$dz = \frac{K}{4}e^{i\Omega}\left[\left(\zeta+\frac{1}{\zeta}\right) - 2\cos(\gamma)\right]\left[1-\frac{1}{\zeta^2}\right]d\zeta \qquad (2.6)$$

$$\text{where} \quad K = \frac{2a^2}{V_\infty}$$

The parametric equations of the free streamlines ℓ_{CD} and ℓ_{EF} are obtained by integrating (2.6) from $\zeta = \pm 1$ to ζ', where ζ' is a point on CB or EF.

On the boundary of Δ, $\zeta = e^{i\sigma}$ and (2.6) becomes:

$$dz = K e^{i\theta} e^{-\tau} \left(\cos(\gamma) - \cos(\sigma)\right) \sin(\sigma) d\sigma \qquad (2.7)$$

Let s be the arc length of z onto $\mathcal{P}$ starting from C , s ∈ [0,L] (L is the length of $\mathcal{P}$).

$$ds = K e^{-\tau} \left|\cos(\gamma) - \cos(\sigma)\right| \sin(\sigma) d\sigma \qquad (2.8)$$

As $\theta(\sigma)$ is unknown, the first problems treated had very simple $\theta(\sigma)$ functions, such as a two-value function for a flat plate or a wedge.

Let β be the angle between the tangent at a point on $\mathcal{P}$ and the x-axis, and ε the one-to-one boundary correspondence function.

$$\varepsilon : \ \sigma \in [0,\pi] \rightarrow \ s \in [0,L]$$

Then, from the geometry of the contour, let us write:

$$\theta(\sigma) = (\beta \circ \varepsilon)(\sigma) - \pi \qquad \forall \sigma \in [0,\gamma[$$
$$\theta(\sigma) = (\beta \circ \varepsilon)(\sigma) \qquad \forall \sigma \in]\gamma,\pi] \qquad (2.9)$$

To solve we just have to define ε from (2.8).

At the stagnation point, Ω presents a singularity which is isolated by expressing :

$$\Omega = \Omega_S + \tilde{\Omega}$$

where Ω_S is a particular solution having the same singularity as Ω.

$$\Omega_S = \theta_S + i\tau_S = -\frac{3\pi}{2} + \gamma + i \log\left(\frac{e^{i\sigma} - e^{i\gamma}}{e^{i\sigma} - e^{-i\gamma}}\right)$$

$$\theta_S = -\frac{\pi}{2} \qquad \forall \sigma \in [0,\gamma[$$

$$\theta_S = \frac{\pi}{2} \qquad \forall \sigma \in]\gamma,\pi]$$

$$\tau_S = \ln\left|\frac{\sin\left(\frac{\sigma-\gamma}{2}\right)}{\sin\left(\frac{\sigma+\gamma}{2}\right)}\right|$$

We must analyze $\tilde{\Omega} = \tilde{\theta} + i\tilde{\tau}$ and now (2.8) can be written as:

$$\varepsilon(\sigma) = K \int_0^{\sigma} \frac{2\sin(\sigma')\sin^2\left(\frac{\sigma'+\gamma}{2}\right)}{e^{\tilde{\tau}(\sigma')}} d\sigma' \qquad (2.10)$$

As θ_S is known, (2.9) gives:

$$\tilde{\theta}(\sigma) = (\beta \circ \varepsilon)(\sigma) - \frac{\pi}{2} \qquad \forall \sigma \in [0,\pi] \qquad (2.11)$$

$\tilde{\tau}$ is calculated using Schwarz-Villat's formula:

$$\tilde{\tau}(\sigma) = \qquad (2.12)$$
$$\frac{1}{\pi} \lim_{\zeta \to e^{i\sigma}} \mathrm{Im}\left\{ \int_0^{\pi} \frac{1-\zeta^2}{1-2\zeta\cos(\sigma')+\zeta^2} \tilde{\theta}(\sigma') d\sigma' \right\}$$

$\Omega(0) = 0$ means $\int_0^{\pi} \theta(\sigma') d\sigma' = 0$ hence

$$\gamma = \frac{\pi}{2} + \frac{1}{\pi} \int_0^{\pi} \tilde{\theta}(\sigma') d\sigma' \qquad (2.13)$$

$\varepsilon(\pi) = L$ allows us to determine K, and we write (2.10) in the form

$$\varepsilon(\sigma) = L\left(\frac{E(\sigma,\gamma)}{E(\pi,\gamma)}\right) \qquad (2.14)$$

$$\text{where } E(\sigma,\gamma) = \int_0^{\sigma} \frac{2\sin(\sigma')\sin^2\left(\frac{\sigma'+\gamma}{2}\right)}{e^{\tilde{\tau}(\sigma')}} d\sigma'$$

The unknowns are functions $\sigma \rightarrow \tilde{\theta}$, $\tilde{\tau}$, ε, and angle γ.

Relations (2.11), (2.12), (2.13), (2.14) supply a functional system of four equations written as :

$$\tilde{\theta} = \mathcal{J}(\varepsilon) \qquad (2.11')$$
$$\gamma = \mathcal{G}(\tilde{\theta}) \qquad (2.12')$$
$$\tilde{\tau} = \mathcal{L}(\tilde{\theta}) \qquad (2.13')$$
$$\varepsilon = \mathcal{E}(\tilde{\tau},\gamma) \qquad (2.14')$$

2.2 Numerical Procedure and Computed Results

The functional system is solved by building, from any initial correspondence function ε_0, a series $\tilde{\theta}_n, \gamma_n, \tilde{\tau}_n, \varepsilon_n$, using the following recursive algorithm:

$$\tilde{\theta}_n = (1-r_\theta)\mathcal{J}(\varepsilon_{n-1}) + r_\theta \tilde{\theta}_{n-1}$$
$$\gamma_n = (1-r_\gamma)\mathcal{G}(\tilde{\theta}_{n-1}) + r_\gamma \gamma_{n-1}$$
$$\tilde{\tau}_n = (1-r_\tau)\mathcal{L}(\tilde{\theta}_{n-1}) + r_\tau \tilde{\tau}_{n-1}$$
$$\varepsilon_n = (1-r_\varepsilon)\mathcal{E}(\tilde{\tau}_{n-1},\gamma_{n-1}) + r_\varepsilon \varepsilon_{n-1}$$

As the existence and uniqueness of the solution has been proved, we consider that the solution is reached if the process converges. Then it is easy to calculate w and thus find the pressure distribution, the drag, and the lift.

In most cases, the number of iterations varies from 10 to 50, corresponding to a few minutes' calculations on a PC 486-DX 50 type computer. The accuracy can be improved by increasing the number of iterations and quadrature points (usually 500 points).

To study obstacles with high curvature the values of the weighting factors to obtain convergence, are: $r_\varepsilon = r_\theta = r_\tau = 0.5$ and $r_\gamma = 0$. For polygonal obstacles, they must be greater.

To test the capacity of our program we compare the C_D and C_L that it computes with the exact values, or values given in the literature. First, we consider

three obstacles with straight boundaries, then obstacles with curved boundaries.

• Inclined plate

This is a geometry whose exact solution is well known. The classical values of C_D, C_L, and γ are:

$$\gamma = \delta + \frac{\pi}{2}, \qquad C_D = \frac{\pi \cos^2(\delta)}{4 + \pi \cos(\delta)},$$

$$\text{and} \qquad C_L = \frac{\pi \cos(\delta) \sin(\delta)}{4 + \pi \cos(\delta)},$$

where δ is the angle between the perpendicular to the wall and the x-axis.

For different values of δ, the values of C_D, C_L, and γ that we computed, reproduce the exact values of C_D, C_L and γ obtained from these formulas.

• Inclined plate with separation on the backface

Let us consider a plate inclined at an angle of 30° with the separation point prescribed in the middle of the back face. This case was studied recently by Elcrat and Trefethen[5]. Their computed values of C_D and C_L are:

$C_D = 0.000575$ $\qquad$ $C_L = 2.26628$

We find :

$C_D = 0.000574$ $\qquad$ $C_L = 2.26652$

• Asymmetrical wedge

The upper face of the wedge is inclined at an angle of 30°, the lower face at 45°, and both faces are the same length. Elcrat and Trefethen[5] computed :

$C_D = 0.33703$ $\qquad$ $C_L = 0.07397$

We find :

$C_D = 0.33707$ $\qquad$ $C_L = 0.07400$

• Circular cylinder

We compare our results to those calculated by Birkhoff and Zarantonello[2], Brodetski, and Schmieden[7].

$\phi = 55.04°$ (angle of separation)

Brodetski	$C_D = 0.500$
Birkhoff et Zarantonello	$C_D = 0.499$
We find	$C_D = 0.4986$

• Convex and concave circular arcs

Our program reproduces the values published by Birkhoff and Zarantonello[2].

• Comparison with experiments

To show that the method described in this paper works for an arbitrary obstacle, we will now present two new Helmholtz's flow calculations and compare them with experimental results.

The first is a NACA 0012 wing section with a 0.2 chord simulated split flap deflected at 60°. The section lift coefficient is given by Abbott and Von Doenhoff [1]. The separation points are placed at the flap extremity and trailing edge. Figure (2.IV) shows as good an agreement with experimental results as Joukowsky's method in the classical theory of wing sections.

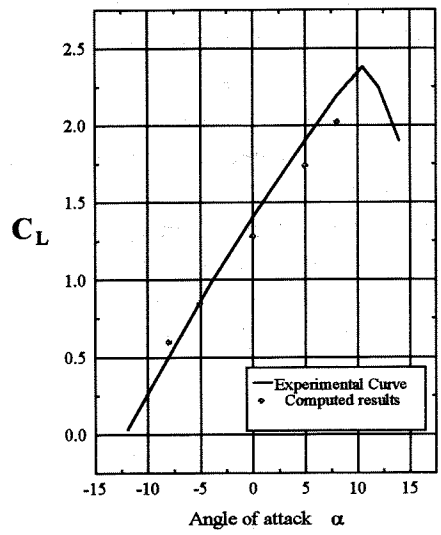

Fig (2.IV)

The second calculation is of a thick wing section with boundary layer suction as used in the Cousteau-Malavard sail of windsail ships. Its surface section consists of a half ellipse upstream and a semi-circle with a flap downstream (Fig (2.V)). As we do not know ϕ, we give it a value so that, when α is zero, the C_L we calculate is equal to the experimental one. Then we assume that the separation point is specified. The results are presented in figure (2.VI). When α is 20°, C_L is computed as ϕ decreases 5°, because prescribing the separation point is not realistic as the angle α increases. This agrees better with experimental results[4].

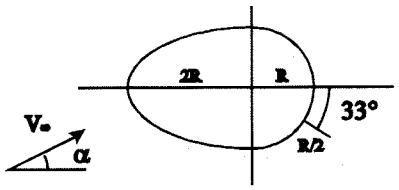

Fig (2.V)

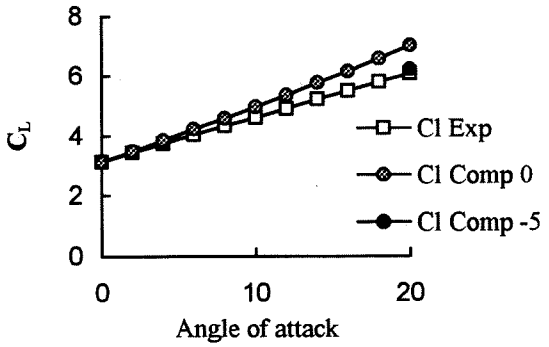

Fig (2.VI)

The results shown in figures (2.IV) and (2.VI) allow us to say that Helmholtz's wake model, in spite of its simplicity, can predict C_L but the C_D values obtained are not realistic because the pressure in the wake generally is not equal to P_∞. To try to improve the drag value, we consider a new model where the pressure in the wake can be $P_0 \neq P_\infty$.

3. The Virtual Wall Model

The virtual wall model proposes, as an innovation, to calculate the wake pressure P_0 or the wake pressure coefficient Cp_0 thanks to an original contribution of the momentum theorem. Releasing the pressure in a wake still considered as a motionless area extending to infinity, is made possible provided that walls separate the wake from the general flow at infinity[6][7][14][18]. The wake is first limited by free streamlines and then limited by virtual walls, so called as they do not appear in the real flow. The locations of the beginning of these walls is also calculated by the model. In this way, the solution is reached without experimental data input and without choice of parameters. Now, let us refer to the figure (3.I). Consider an obstacle in an infinite stream of velocity V_∞, parallel to the x-axis, and of pressure P_∞. The Bernoulli theorem applies between the point at infinity upstream and a point of a free streamline, which links P_0 and P_∞.

A is the stagnation point. F and B are respectively the lower and upper separation points, specified as in the previous model. The arc FB represents the wetted wall, so called $\mathcal{P}$. The free streamlines ℓ_{BC} and ℓ_{FE} join the separation points to the beginning of the virtual walls. CD and ED represent the horizontal virtual walls running to infinity. These are not only lines of discontinuity for the velocity (like free streamlines) but also for the pressure. On CD and ED, outside the wake, the pressure of the flow tends to P_∞.

The boundary conditions for the complex velocity w are written as follows

$$\begin{cases} \lim\limits_{|z|\to\infty} w = V_\infty \\ \mathrm{Im}\{wdz\} = 0 \text{ on } \mathcal{P}, CD, ED \\ |w| = V_0 \qquad \text{on } \ell_{BC}, \ell_{FE} \end{cases} \tag{3.1}$$

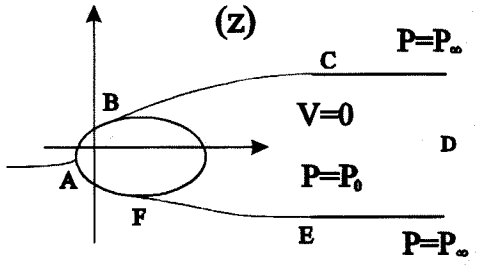

fig (3.I)

3.1 Theoretical Formulation

The technique of resolution that is used then is quite similar to that used in Helmholtz's model, considering the log-hodograph function

$$Q(\zeta) = \mathrm{Log}\frac{V_\infty}{w(\zeta)} = T(\zeta) + i\Theta(\zeta) \tag{3.2}$$

with, now $|\vec{V}| = V_\infty e^{-T}$. It is usual to write, on the unit circle

$$\begin{cases} T(\zeta) = T(e^{i\sigma}) = \tau(\sigma) \\ \Theta(\zeta) = \Theta(e^{i\sigma}) = \theta(\sigma) \end{cases} \tag{3.3}$$

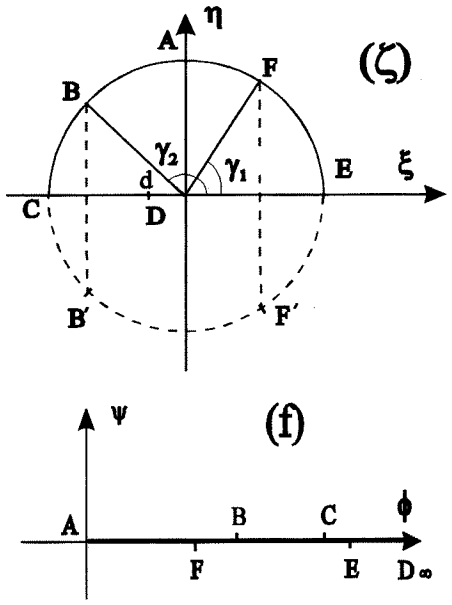

fig (3.II)

Levi-Civita's method still applies, particularly consisting in mapping the flow inside the upper half Δ^+ of the unit disk Δ. The choice of the function Q instead of Ω proceeds from the principle of reflexion requiring the function to be real on the real diameter. Indeed, contrary to the previous model, it is convenient that the real diameter of the auxiliary plane figures the virtual walls of the physical plane (instead of the free streamlines) where the argument of the velocity vanishes. Moreover, this process removes the

virtual walls from the resolution (still justifying its name). The mixed problem is simplified as it gets a symmetry across the real axis. But it does not degenerate in a Dirichlet problem as in the Helmholtz model. We are then led to solve, in the whole disk, a four-arc mixed problem for Q.

Figure (3.II) shows both potential and auxiliary planes.

On ℓ_{BC} and ℓ_{FE}, function τ is known as soon as Cp_0 is calculated. On $\mathcal{P}$, function $\theta(\sigma)$ defined as

$$\begin{cases} \theta(\sigma) = (\beta \circ \varepsilon)(\sigma) - \pi & \text{on } \left[\gamma_1, \frac{\pi}{2}\right[\\ \theta(\sigma) = (\beta \circ \varepsilon)(\sigma) & \text{on } \left]\frac{\pi}{2}, \gamma_2\right] \end{cases} \tag{3.4}$$

is known as soon as $\varepsilon(\sigma)$

$$\varepsilon: \quad \sigma \in [\gamma_1, \gamma_2] \quad \rightarrow \quad s \in [0, L] \tag{3.5}$$

is calculated. s is the arc length of z onto $\mathcal{P}$ starting from F, and L is the length of $\mathcal{P}$. β always means the angle between the tangent and the x-axis.

As previously, in order to get a continuous function, the stagnation point singularity is eliminated putting

$$\tilde{Q}(\zeta) = Q(\zeta) - Q_s(\zeta) \tag{3.6}$$

where

$$Q_s(\zeta) = -\mathrm{Log}(\zeta - i)(\zeta + i) \tag{3.7}$$

The solution to the mixed problem for $\tilde{Q}$ is then given by the integral[13]

$$\tilde{Q}(\zeta) = \frac{X(\zeta)}{i\pi} \int_{L'} \frac{\tilde{T}(t)dt}{X(t)(t-\zeta)} + \frac{X(\zeta)}{\pi} \int_{L''} \frac{\tilde{\Theta}(t)dt}{X(t)(t-\zeta)} \tag{3.8}$$

with

L'=F'EF∪BCB' L''=FAB∪B'A'F'

and

$$X(\zeta) = \sqrt{\left(\zeta - e^{i\gamma_1}\right)\left(\zeta - e^{i\gamma_2}\right)\left(\zeta - e^{i(2\pi-\gamma_2)}\right)\left(\zeta - e^{i(2\pi-\gamma_1)}\right)} \tag{3.9}$$

Note that there is a condition of existence for the mathematical mixed problem[13] that must be verified by the solution, namely

$$\int_{L'} \frac{\tilde{T}(t)dt}{X(t)} + i \int_{L''} \frac{\tilde{\Theta}(t)dt}{X(t)} = 0 \tag{3.10}$$

The study is then complete considering the following function which conformally maps ζ-plane on f-plane

$$f(\zeta) = \frac{f_E f_C \left(\zeta + \frac{1}{\zeta}\right)^2}{\left[\sqrt{f_E} - \sqrt{f_C} - \frac{1}{2}\left(\zeta + \frac{1}{\zeta}\right)\left(\sqrt{f_E} + \sqrt{f_C}\right)\right]^2} \tag{3.11}$$

where f_E and f_C mean the affixes of points E and C in the f-plane. Successive steps of mapping occuring in (3.11) have been avoided because of their similarity with those of the Helmholtz model.

Hence three positions are unknown in the ζ-plane: points B and F, respectively of arguments γ_1 and γ_2, and d, the affix of D, which is related to f_E and f_C by

$$\frac{2d}{d^2+1} = \frac{\sqrt{f_E} + \sqrt{f_C}}{\sqrt{f_E} - \sqrt{f_C}} \tag{3.12}$$

Building the flow field in the physical plane derives then from

$$dz = \frac{df}{w} \tag{3.13}$$

that is

$$dz = 2Ke^{\tau}e^{i\theta} \frac{\left(\zeta^2 - 1\right)\left(\zeta^{-2} + 1\right)}{\left[1 - \frac{d}{d^2+1}\left(\zeta + \frac{1}{\zeta}\right)\right]^3} d\zeta \tag{3.14}$$

where, apart from d, appears the unknown coefficient

$$K = \frac{f_E f_C}{V_\infty \left(\sqrt{f_E} - \sqrt{f_C}\right)^2} \tag{3.15}$$

(3.14) is used on the virtual walls, so by integrating from ζ=-1 and from ζ=1 on the real diameter for CD and ED respectively.

On the circle, (3.14) becomes, setting in it $\zeta = e^{i\sigma}$

$$dz = 4Ke^{\tau}e^{i\theta}\left(\frac{\cos\sigma}{\cos\sigma - \frac{d^2+1}{2d}} - 1\right)\frac{\sin 2\sigma}{\left(1 - \frac{2d\cos\sigma}{d^2+1}\right)^2} d\sigma \tag{3.16}$$

Drawing the free streamlines ℓ_{FE} and ℓ_{BC} proceeds from the integration from $\sigma = \gamma_1$ to $\sigma = 0$ and from $\sigma = \gamma_2$ to $\sigma = \pi$. The arc length s is then given by

$$ds = 4e^{\tau}K\left|\left(\frac{\cos\sigma}{\cos\sigma - \frac{d^2+1}{2d}} - 1\right)\frac{\sin 2\sigma}{\left(1 - \frac{2d\cos\sigma}{d^2+1}\right)^2}\right| d\sigma \tag{3.17}$$

Coefficient K is calculated by the integration of ds from $\sigma = \gamma_1$ to $\sigma = \gamma_2$ knowing L.

At this stage of the study, one can list and number the unknowns to determine:

1- the function $\theta(\sigma)$ (or $\tilde{\theta}(\sigma)$) on L'

2- the function $\tau(\sigma)$ (or $\tilde{\tau}(\sigma)$) on L''

3- the one-to-one correspondence $\varepsilon(\sigma)$

4- Cp_0

5,6,7- the variables d, γ_1, γ_2

Functions θ and τ are given by (3.8), while bijection ε is obtained by (3.17) once K has been determined. Position d is clearly determined by the infinity condition of (3.1), say

$$\tilde{Q}(d) + \mathrm{Log}(d^2 + 1) = 0 \qquad (3.18)$$

Equation (3.10) is then related to one of the two unknowns γ_1 or γ_2.

We are now going to see how the application of the momentum theorem supplies two new equations. Let us have a look at figure (3.III) showing the surface reference S chosen for this calculation.

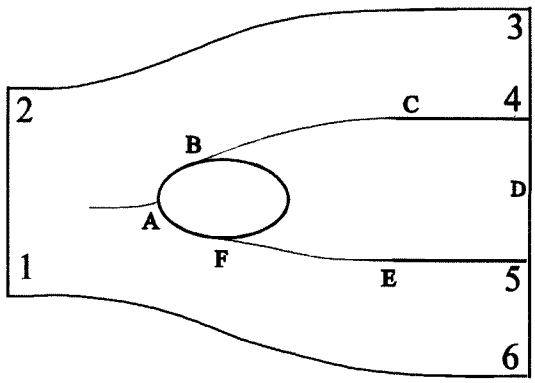

fig (3.III)

Contour 1-2-3-4-5-6-1 is defined so that boundaries 2-3 and 1-6 are streamlines at pressure P_∞ and velocity V_∞. Segments 1-2, 3-4 and 5-6 are considered sufficiently far upstream and downstream to assume that $\vec{V} = V_\infty \vec{x}$. Writing the momentum theorem leads to:

$$\int_S \rho \vec{V}(\vec{V}.\vec{n})ds = -\vec{R} + \vec{F}_{pressure} \qquad (3.19)$$

where vector $\vec{R}$ is the resultant of the dynamic forces on the body.

With the above choices for S and the law of conservation of mass, it is easily seen that the left hand side of (3.19) vanishes. Finally, after some calculations, one obtains for drag and lift coefficients

$$\lambda C_D = -hCp_0 \qquad (3.20)$$

$$\lambda C_L = \int_C^D Cpdx - \int_E^D Cpdx + Cp_0(x_C - x_E) \qquad (3.21)$$

where $h = y_C - y_E$ is the height between the virtual walls and λ is the reference length of the body (the chord for a wing section) and Cp is the pressure coefficient.

One has to consider that the integrals occurring in formula (3.21) are to be performed in the ζ-plane, and more precisely on the circle diameter up to d. In the same way, the affixes z_C and z_E, required not only for $(x_C - x_E)$ but also for h proceed from (3.16). Equation (3.20) gives the wake underpressure coefficient after the determination of h and the integration of the pressure coefficient on the wall of the obstacle (for C_D), while (3.21) is related to one of the arguments γ_1 or γ_2 (occurring, in the integrals, as an end of the path of integration).

Hence, we get a system of seven equations (3.8) twice, (3.10), (3.17), (3.18), (3.20) and (3.21) in order to determine the seven unknowns.

3.2 Numerical Procedure and Computed Results

Taking into account the symmetry due to the principle of reflexion, the integral occurring in (3.8) can be reduced to the half upper of the unit circle. The calculation is however difficult to perform because of the two singularities $e^{i\gamma_1}$ and $e^{i\gamma_2}$ lying on the path of integration. A classical quadrature -even if the clustering is increased near the singularities- does not meet the case as a good accuracy is not reached.

Therefore, a numerical method has been elaborated and tried on test functions[9]. It consists in finding a primitive either to a piece or the whole (in symmetrical flow configurations) of the integrable part of the function lying under the integral, the other part being taken at the middle of the integration segment.

If a constant partition lower than 0.5 degree is chosen, this method proves its ability to calculate accurately the solution all along the circle, including the points lying near the discontinuities. Relative error does not exceed 1% if we exclude the points where the function vanishes.

Now, in order to solve the seven- unknown above system, we have to build a series

$$\left\{\varepsilon_n, \tilde{\tau}_n, \tilde{\theta}_n, Cp_{0(n)}, \gamma_{1(n)}, \gamma_{2(n)}, d_n\right\}$$

using a relaxed iterative algorithm. To start, only initial guesses for Cp_0, γ_1 and function $\varepsilon(\sigma)$ have to be specified. In most of the symmetrical cases, the convergence is reached after 30 to 50 iterations, requiring a few minutes' calculation on an IBM RISC 6000 (27 MIPS).

We built first a simplified program which only applies to symmetrical flows. In this way, because of the symmetry, only one of the two arguments γ_1 or γ_2 is unknown, say γ_1, and, moreover, d=0. According to these two unknowns, equations

(3.10) and (3.21) disappear in the system of equations as they are always verified.

With a function ε taken as linear, and any initial choices for Cp_0, γ_1, calculations have been performed and a solution reached for a wedge with $\pi/2$ apex angle and edge rounded off (which makes it look like real body), a 2:1 elliptic cylinder and the circular cylinder for separation angle up to 110°.

For the flat plate perpendicular to the wind and the circular cylinder with a separation angle greater than 110°, convergence is difficult to reach with the above initialisation. Anyway, a further study of the conditions of existence and uniqueness would help to understand.

Concerning circular cylinder (λ=cylinder diameter), calculation is presented for 75° separation angle, as it is close to the separation angle experimentally occuring in subcritical range. Figure (3.IV) shows the fairly good agreement found between computed and experimental pressure distributions.

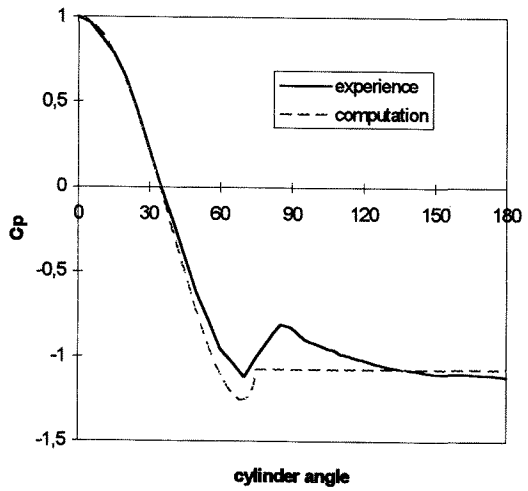

fig (3.IV)

Computation gives:

$C_D = 1.13$ $Cp_0 = -1.07$

compared to experimental values[15]

$C_D \cong 1.2$ $Cp_0 \cong -1.1$

Increasing separation angle value shows increasing progressive accordance with Helmholtz's model values. It seems that the two models hold the same limit case of zero drag which lies at 124.21°.

2:1 elliptic cylinder has also been investigated (λ=minor axis). Two calculations have been performed for 10° and 0° tangent angles at separation.

10° comp. values:

$C_D = 0.73$ $Cp_0 = -0.03$

0° comp. values:

$C_D = 0.36$ $Cp_0 = -0.1$

Experimentally, in subcritical range, considering a separation angle within the interval [0°,10°], $C_D \cong 0.6$[17].

The general program has been written in order to compute dissymetrical flows. A strong dependence on the condition of existence has been shown up. Indeed, if this is not verified, computed values of variables no longer make sense. For example, τ values on the real diameter of ζ-plane near -1 and 1 do not connect the prescribed values in these points. Consequently, the building of the series

$$\left\{\varepsilon_n, \tilde{\tau}_n, \tilde{\theta}_n, Cp_{0(n)}, \gamma_{1(n)}, \gamma_{2(n)}, d_n\right\}$$

is more difficult than in the case of symetrical flow, and no exact convergence has yet been reached. An optimisation of both conditions of initialisations and choices of relaxation coefficients is carrying out.

4. Conclusion

Inside the wing section theory, our works, concerning 2D-thick wake modelling, can be seen as coming on top of earlier studies about thin wakes, in steady cases, that is Joukowsky's theory, or in unsteady cases, that is Couchet-Mudry's theory. Because of their generality and agreements found between computed and experimental values, both models -Helmholtz's and the Virtual Wall one- can be clearly considered as good prediction tools. They produce evidence that using powerful developments of complex analysis is always an interesting challenge in fluid dynamics modelling.

However, one can argue that representing the wake by a motionless area is certainly a crude modelling of turbulent and viscous effects experimentally occurring. We cannot reasonably put forward objections to that, but our purpose is not to become a serious threat to Computational Fluid Dynamics. Indeed, these models must rather be considered as basic models, with regard both to their relative theoretical simplicity and economical computation time. Quick results can be obtained either to give a first idea on a phenomenon, or to have initial guesses for a CFD code.

The fact remains nonetheless that one can justify their attractive aspect by accounting for their autonomy where no parameter appears and no experimental value is required. For several bodies, taking into account a coupling procedure with a boundary layer calculation -to determine separation points-, Helmholtz's model predicts lift and the Virtual Wall model predicts drag but also wake pressure. The Dissymetrical Virtual Wall model, still numerically studied at the moment, should supply a complete prediction. Further investigations will carry us through to a successful conclusion, but if convergence cannot be reached, the existence of solution, that we do not take into account, will be studied.

References

[1] Abbott and A. E. Von Doenhoff :
Theory of wing section. Dover publication 1958.

[2] G. Birkhoff and E. H. Zarantonello :
Jets, Wakes, and Cavities. Academic press 1957.

[3] G. Couchet :
Les profils en aérodynamique instationnaire et la condition de Joukowsky. Lib. scient. et tech. A. Blanchard 1976.

[4] A. Daif et M. Mudry :
L'aérodynamique des profils épais aspirés. *7eme congrès français de mécanique*. 1985.

[5] A. R. Elcrat and L. N. Trefethen :
Classical free streamline flow over a polygonal obstacle. *J. Comput. Appl. Math*. 14. 1986.

[6] R. Eppler :
Beiträge zu Theorie und Anwendung der unstetigen Strömungen. *J. Ratl. Mech. Anal*., 3, pp. 591-644, 1954.

[7] M. I. Gurevich :
The theory of jet in an ideal fluid. Pergamon press 1966.

[8] J. Hureau :
La transformation conforme et l'étude numérique d'écoulements stationnaires ou instationnaires autour d'obstacles avec sillage. *Thèse Orléans* 1988.

[9] Ph. Legallais :
Le problème mixte et la modélisation d'écoulements autour d'obstacles avec sillage. *Thèse Orléans* 1994.

[10] T. Levi-Civita :
Scie e leggi di resistenzia. *Rendiconti del circolo Mathematico di Palermo* Tome 23 1907.

[11] J. Leray :
Les problèmes de représentation conforme d'Helmholtz, théories des sillages et des proues. *Comentaru Mathematici Helvetici* Tome 8 1935-36.

[12] M. Mudry :
La théorie générale des nappes et filaments tourbillonnaires et ses applications à l'aérodynamique instationnaire. *Thèse d'état, Paris VI*, 1982.

[13] N.I. Muskhelishvili :
Singular integral equations. Noordhoff International Publishing 1977.

[14] A. Roshko :
A new hodograph for free streamline theory, NACA TN 3168, 1954.

[15] H. Schlichting :
Boundary layer theory. Mc Graw Hill, 1968.

[16] H. Villat :
Sur la résistance des fluides. *Thèse Paris* 1911. *Leçons sur l'hydrodynamique*, Gauthier-Villars 1929.

[17] F. M. White :
Fluid Mechanics. Mc Graw Hill, 1986.

[18] T. Y. Wu :
Inviscid cavity and wake flows, in *Basic developments in fluid dynamics*. M. Holt ed. Academic Press 1968.